

SEG-SAM: Semantic-Guided SAM for Unified Medical Image Segmentation

Shuangping Huang¹, Hao Liang¹, Qingfeng Wang¹, Chulong Zhong¹, Zijian Zhou², Miaoqing Shi^{3*}
¹South China University of Technology, ²King’s College London, ³Tongji University

eehsp@scut.edu.cn, eelhlyf@mail.scut.edu.cn, mshi@tongji.edu.cn

Abstract

Recently, developing unified medical image segmentation models gains increasing attention, especially with the advent of the Segment Anything Model (SAM). SAM has shown promising binary segmentation performance in natural domains, however, transferring it to the medical domain remains challenging, as medical images often possess substantial inter-category overlaps. To address this, we propose the SEmantic-Guided SAM (SEG-SAM), a unified medical segmentation model that incorporates semantic medical knowledge to enhance medical segmentation performance. First, to avoid the potential conflict between binary and semantic predictions, we introduce a semantic-aware decoder independent of SAM’s original decoder, specialized for both semantic segmentation on the prompted object and classification on unprompted objects in images. To further enhance the model’s semantic understanding, we solicit key characteristics of medical categories from large language models and incorporate them into SEG-SAM through a text-to-vision semantic module, adaptively transferring the language information into the visual segmentation task. In the end, we introduce the cross-mask spatial alignment strategy to encourage greater overlap between the predicted masks from SEG-SAM’s two decoders, thereby benefiting both predictions. Extensive experiments demonstrate that SEG-SAM outperforms state-of-the-art SAM-based methods in unified binary medical segmentation and task-specific methods in semantic medical segmentation, showcasing promising results and potential for broader medical applications.

1. Introduction

Medical image segmentation aims to segment regions of interest in medical images, playing a vital role for medical analysis and clinical diagnosis [10, 15, 27, 44]. The segmentation tasks can involve various image modalities (e.g., CT, MRI, and X-rays) and medical structures, (e.g., organs and tissues). This diversity makes developing a specific

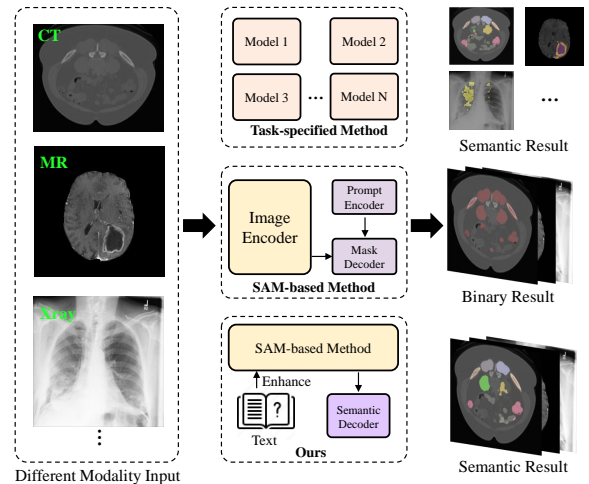


Figure 1. The comparison of our SEG-SAM with task-specific and SAM-based methods for medical image segmentation. In the former, each image modality is processed by a separate model. In the latter, all image modalities are handled in a unified manner, but the model can only produce binary masks. Distinct from both, our method leverages semantic learning and text knowledge to achieve unified semantic mask prediction.

model for each task is both complex and labor-intensive. Therefore, effectively handling medical segmentation in a unified manner is gaining increasing attentions.

To perform unified medical segmentation, a common practice is to train a deep neural network from various medical data [3, 36, 39]. However, this requires carefully designed modules to handle inherent differences across data sources. Recently, the Segment Anything Model (SAM) [22] shows promising segmentation performance in the natural domain with specifically crafted interactive prompts (e.g., points, bounding boxes) as guidance, which paves a new way for unified medical segmentation. Among them, MedSAM [28] does a vanilla fine-tuning of SAM on medical data to transfer the pre-trained knowledge from the natural into medical domain. Following this, Med2D [45] and SAM-SP [40] use parameter-efficient fine-tuning and knowledge distillation techniques (e.g., adapter [9]) to

*Corresponding author

equip the model with medical knowledge. However, like SAM, the interactive prompts in these methods are focused on concrete objects for binary segmentation while the semantic attributes (*e.g.*, object categories) are overlooked. Category-specific semantics is crucial for unified medical segmentation, as medical images often possess heavier inter-category overlaps than natural images. For instance, in order to accurately distinguish between the liver and kidney, which are visually alike and spatially adjacent, we would need to rely on not only point-based prompts but also the semantic differences between them.

The observation inspires us to incorporate the semantic learning into SAM to facilitate unified medical segmentation. It is, however, not straightforward to fine-tune the pre-trained SAM with semantic medical labels, owing to the potential conflict between binary and semantic segmentation. Therefore, we integrate a semantic-aware decoder (SAWD) independent of SAM’s original semantic-agonistic decoder (SAGD) to learn specialized semantic knowledge in medical categories. To this end, we initialize a segmentation-oriented token in the SAWD, which, by interacting with SAM’s image features and visual prompts, directly decodes semantic segmentation on the prompted object; also, a set of classification-oriented tokens, which, by interacting with image features but ignoring visual prompts, decode the classification results on those unprompted objects. The latter, without drifting too much from the model’s focus on the prompted object, guides it to precisely segment the prompted object boundaries. In addition, to further enhance the model’s semantic understanding, we integrate the medical text descriptions into the model inspired by text promptable segmentation [22, 44]. We obtain key characteristics of medical object categories by the LLM and encode them into text embeddings. To incorporate medical text knowledge into our method, we develop a text-to-vision semantic enhancement scheme, enabling interactions between text and vision embeddings. A specialized text summary token is appended after the text embeddings to summarize the text knowledge, and then is combined with visual prompts tokens. This text-to-vision interaction allows the model to explore comprehensive text knowledge across medical categories, enabling it to adaptively focus on the prompted object’s representation for its segmentation.

Finally, given the prompted object, the SAWD’s prediction tends to focus on the semantic difference between categories while the SAGD’s on the foreground-background difference in a certain image. They have different focuses yet are also complementary. Therefore, we establish the consistency between the segmentation masks respectively produced from two decoders. To do this, we propose a cross-mask spatial alignment to encourage the outputs from SAWD and SAGD to have more overlap, benefiting for the predictions of both.

To the best of our knowledge, we are the first to introduce the semantic learning into SAM to achieve unified medical semantic segmentation. We name the proposed unified medical segmentation model as **SEmantic-Guided SAM (SEG-SAM)** (see Fig. 1). Extensive experiments on various publicly available datasets demonstrate that the proposed SEG-SAM outperforms other SAM-based models on binary medical segmentation, while offering additional benefits on semantic prediction. Additionally, we evaluate the semantic medical segmentation performance between our method and state-of-the-art conventional methods, showcasing promising results and potential for wider medical application.

2. Related Work

Medical Image Segmentation. With the development of deep neural networks (DNNs), medical image segmentation has achieved significant progress. The FCN [26] is the first to introduce a fully convolutional architecture for end-to-end image segmentation. Following this, U-Net [32] stands as one of the most successful medical image segmentation methods, which utilizes the skip connections on top of the encoder-decoder to learn multi-scale features. Subsequently, the U-Net family [1, 2, 19] incorporates various model components (*e.g.*, effective re-sampling strategies and feature extraction modules) to address different medical challenges. With the rise of Transformer [13, 25, 33] in computer vision, many methods [5, 7] integrate it into the U-shaped architecture to facilitate the robust visual feature extraction. All these methods, despite with excellent performance, are task-specific and not generalizable across tasks.

Recently, an increasing number of studies is devoted into the unified semantic medical segmentation to simultaneously handle multiple medical datasets [4, 24, 37]. UniSeg [37] integrates multiple datasets to train the model to understand the correlations across datasets. UniverSeg [4] leverages the across-dataset image pairs to achieve the unified segmentation model, allowing for new task generalization without the need of finetuning. HermesNet [14] integrates task and modality priors of medical images to achieve modality prediction by attention mechanism, thus reducing the image heterogeneity. Although these methods achieve unified medical segmentation, they require explicit design to handle the domain gaps across datasets, till the introduction of Segment Anything Model (SAM), specified below.

SAM in Medical Image Segmentation. SAM employs interactive prompts to effectively perform binary mask prediction of diverse objects, leveraging large-scale image pre-training. Later, a series of efforts have been made to extend it to specialized domains [6, 20, 31, 38]. Amongst them, when applying SAM to the medical domain, model fine-tuning on medical images is normally required due to the large domain gap. To achieve this, MedSAM [28] and

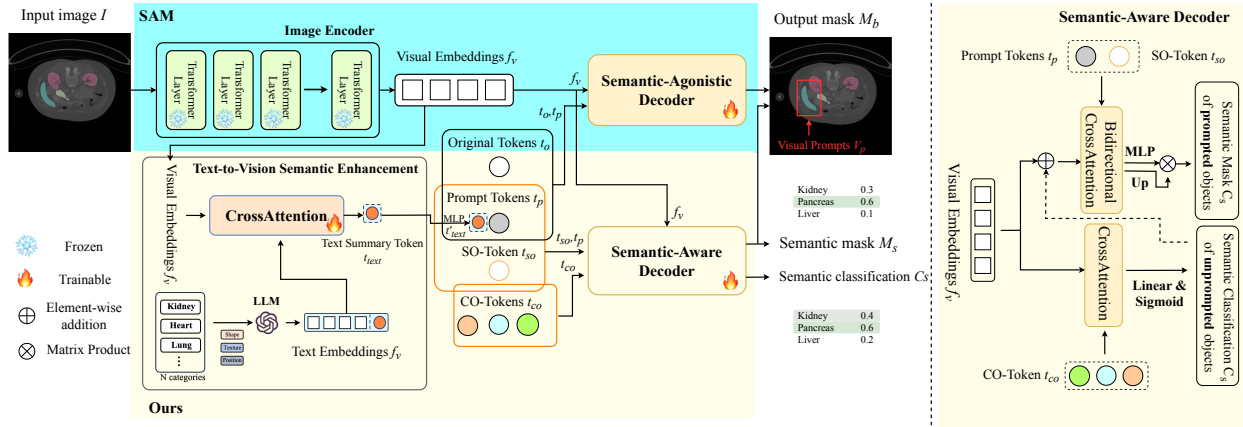


Figure 2. Overview of the SEG-SAM framework. Given an image I with the prompted object O_p from visual prompts V_p , first, SAM’s image encoder extracts visual embeddings f_v , while the prompt encoder encodes V_p into prompt tokens t_p . Next, SAM’s original decoder uses the original tokens t_o to predict binary masks \hat{M}_b for O_p . Then, our proposed semantic-aware decoder uses a segmentation-oriented token t_{so} to predict the semantic mask \hat{M}_s for O_p and classification-oriented tokens t_{co} to capture category information of unprompted objects. Lastly, medical text descriptions generated from a pre-trained LLM are incorporated into the text summary token t_{text} through a text-to-vision semantic enhancement scheme, and t_{text} is embedded into the prompt tokens t_p to improve segmentation performance.

SAM-Med2D [12] introduces large-scale medical datasets to fine-tune SAM for transferring its knowledge to medical tasks. Furthermore, Medical SAM-Adapter [34] introduces two dedicated modules, the space-depth transpose and hyper-prompting, for effectively adapting SAM to the 3D medical segmentation. SAM-SP [41] introduces a self-prompting scheme to improve object mask prediction and further enhances the segmentation performance through knowledge distillation between generated masks. Notwithstanding these progress, they are still confined to binary segmentation due to SAM’s prompting architecture. Recently, MaskSAM [35] introduces the category-based prompt generator, refining SAM’s original visual prompts to incorporate category information, thus achieving semantic medical segmentation. However, they turn the unified binary segmentation into the task-specific semantic medical segmentation, hence are incapable of generalizing across tasks.

3. Method

We begin by reviewing the SAM [22] architecture; then, introduce our SEG-SAM for unified medical image segmentation; lastly, we describe SEG-SAM’s loss function, training and inference strategies.

3.1. Preliminary: SAM

SAM [22] is proposed to perform image segmentation with interactive prompts, which primarily consists of three basic components: 1) an image encoder Enc_{img} which employs a vision transformer (ViT) [13] as backbone to extract visual embeddings f_v from the input image I ; 2) a prompt encoder

Enc_{pmt} which encodes the visual prompts V_p (*i.e.*, points and bounding boxes) as prompt tokens t_p to guide the model for object segmentation; and 3) a semantic-agnostic decoder Dec_{sag} which leverages the attention mechanism to achieve interaction between the visual embeddings f_v , the prompt tokens t_p , and a set of learnable tokens t_o , for binary mask prediction. After Dec_{sag} , the refined visual embeddings f'_v are upsampled and multiplied with refined learnable tokens t'_o to generate the final binary masks \hat{M}_s .

3.2. Semantic-Guided SAM

The proposed SEG-SAM framework retains SAM’s original design to preserve its representational capability, while introducing additional semantic learning. As shown in Fig. 2, given an image $I \in \mathbb{R}^{3 \times H \times W}$ with the prompted object O_p from visual prompts V_p (*i.e.*, points and bounding boxes), we employ SAM’s image encoder Enc_{img} to extract visual embeddings $f_v \in \mathbb{R}^{D \times \frac{H}{p} \times \frac{W}{p}}$ and prompt encoder Enc_{pmt} to encode visual prompt V_p as prompt tokens $t_p \in \mathbb{R}^{L \times D}$, where D is the feature dimension, p is the patch size, and L is the number of point prompts (the box can be seen as two corner points), specified below:

$$f_v = \text{Enc}_{\text{img}}(I), t_p = \text{Enc}_{\text{pmt}}(V_p). \quad (1)$$

After obtaining f_v and t_p , we retain SAM’s original semantic-agnostic decoder Dec_{sag} , which utilizes learnable tokens t_o to predict the binary mask \hat{M}_b for the prompted object O_p . To further introduce semantic learning, we propose a semantic-aware decoder Dec_{saw} for semantic prediction. Specifically, we initialize an segmentation-oriented to-

ken t_{so} in Dec_{sag} to predict the semantic mask \hat{M}_s of O_p . In addition, we initialize a set of classification-oriented tokens t_{co} to capture category-specific information of unprompted objects in the image, so as to help the accurate mask prediction on O_p . Instead of segmenting masks for unprompted objects, we focus on predicting their categories, reducing computational overhead and avoiding potential conflict with segmentation of the prompted object (Sec. 3.2.1). To further enhance the model’s semantic understanding, we solicit medical text descriptions D_{text} from the LLM and develop the text-to-vision semantic enhancement (T2VSE) scheme, which incorporates fine-grained medical knowledge into the model’s prompt tokens t_p (Sec. 3.2.2). The overall process can be specified below:

$$t'_p = \text{T2VSE}(f_v, t_p, D_{\text{text}}), \quad (2)$$

$$\hat{M}_b = \text{Dec}_{\text{sag}}(t_o, t'_p, f_v), \quad (3)$$

$$\hat{M}_s, \hat{C}_s = \text{Dec}_{\text{saw}}(t_{so}, t_{co}, t_p, f_v). \quad (4)$$

Next, we detail two key components of the proposed SEG-SAM, *i.e.*, the semantic-aware decoder and text-to-vision semantic enhancement scheme.

3.2.1 Semantic-Aware Decoder

While visual prompts provide concrete spatial location to segment certain objects, medical images present unique challenges: the frequent inter-class overlap and blurred spatial boundaries between objects can lead to ambiguous binary masks. To address this, we introduce explicit semantic learning into SAM. Nevertheless, performing binary and semantic predictions concurrently can lead to potential conflicts. To overcome it, we propose a semantic-aware decoder Dec_{saw} for semantic prediction instead of reusing SAM’s original decoder. As shown in Fig. 2, Dec_{saw} produces semantic mask P_{mask} for the prompted object O_p and auxiliary semantic category predictions P_{cat} for other unprompted objects, specified below.

Semantic mask prediction for prompted object. We begin by defining the ground-truth semantic masks M_s to replace original binary masks M_b in unified datasets. Specifically, for all binary masks, each is associated with a unique semantic category, allowing us to construct the overall semantic masks, *i.e.*, $M_s = [C_s, M_b]$. Next, we initialize a learnable token in Dec_{saw} , namely the semantic-oriented token (SO-Token) t_{so} , to decode the semantic information of prompted object O_p . Given the prompt tokens t_p in Enc_{pmt} and visual embeddings f_v in Enc_{img} , Dec_{saw} leverages the attention mechanism (detailed later) to perform the feature interaction among the SA-Token t_{so} , t_p and f_v , enabling the prediction of semantic mask \hat{M}_s for prompted object O_p .

“Each binary mask is associated with a unique category label, allowing us to construct an overall semantic mask.”

Semantic classification for unprompted objects. Intuitively, apart from the prompted object, we can also incorporate the semantic segmentation on unprompted objects to perform full-image semantic segmentation. However, we observe that this can drift the model’s focus from visual prompted object to unprompted objects in the image thus affecting the gradient updates for prompted one, putting aside the unnecessary complexity and computational overhead in this process. As our primary goal is to accurately segment the prompted object, we simplify the learning process by only performing semantic classification P_{cat} in Dec_{saw} on those unprompted objects. In this way, the semantic segmentation task on the prompted object becomes the main task, occupying the main endeavors of the learning. Specifically, we initialize N classification-oriented tokens (CO-Tokens) t_{co} for unprompted object predictions. Each CO-Token is used for an independent binary classification. The Dec_{saw} utilizes a paralleled attention-based branch (specified later) to establish feature interaction between the visual embeddings f_v and CO-Tokens t_{co} . Each CO-Token is appended with a linear layer responsible for predicting binary classification of a certain class on the unprompted objects. Afterwards, we integrate the classification results \hat{C}_s from P_{cat} into SO-Token t_{so} to provide the category-specific prior knowledge. To do this, we apply an MLP to \hat{C}_s and fuse it with SO-Token t_{so} by element-wise addition.

Semantic-aware decoder structure. Given the prompt tokens t_p from Enc_{pmt} and visual embeddings f_v from Enc_{img} , Dec_{saw} consists of dual branches with attention mechanism [33], each of which is designed to establish interaction with different learnable tokens. For the semantic mask prediction P_{mask} of the prompted object O_p , we first concatenate the SA-Token t_{so} and prompt tokens t_p , and employ a self-attention layer to achieve their interaction. Then, we apply the bidirectional cross-attention layers to refine both the concatenated tokens $[t_{so}, t_p]$ and visual embeddings f'_v for generating the semantic mask \hat{M}_s :

$$t'_{so}, f'_v = \text{BiCrossAttn}(\text{SelfAttn}([t_{so}, t_p]), f_v), \quad (5)$$

$$\hat{M}_s = \text{MLP}(t'_{so}) \times f'_v. \quad (6)$$

For the semantic classification P_{cat} of unprompted objects in the image, we use the self-attention followed by cross-attention layer to refine CO-Tokens t'_{co} to predict the classification results \hat{C}_s :

$$t'_{co} = \text{CrossAttn}(\text{SelfAttn}(t_{co}), f_v), \quad (7)$$

$$\hat{C}_s = \text{Sigmoid}(\text{Linear}(t'_{co})), \quad (8)$$

3.2.2 Text-to-Vision Semantic Enhancement

To further enhance the model’s semantic understanding, we incorporate medical text descriptions to help the model

grasp fine-grained medical knowledge. Our motivation is to let medical descriptions capture key characteristics of all medical categories. To achieve this, we utilize the large language model (LLM), *i.e.*, ChatGPT [1], to generate the descriptions $D_{text} \in \mathbb{R}^N$. We construct a generic text template applicable to all object classes, guiding the LLM to specifically focusing on attributes including shape, texture, and positional information. Please refer the template in the supplementary material.

Once obtaining the text description D_{text} , we develop a text-to-vision semantic enhancement scheme. Specifically, we first encode the text description D_{text} into text embeddings $f_t \in \mathbb{R}^{N \times D}$ by ChatGPT’s embedding service. Based on it, we initialize a text summary token t_{text} and concatenate it with f_t . We employ a self-attention layer on the concatenated $[f_t, t_{text}]$ to perform their interaction, so as to transfer the text information to t_{text} . Next, given the visual embeddings f_v in Enc_{img} and prompt tokens t_p in Enc_{pmt} , we use the cross-attention layer to further achieve text-vision interaction, where text embeddings $[f_t, t_{text}]$ are used as the query, and visual embeddings f_v are used as the key and value. This process can be expressed as:

$$t'_{text} = \text{CrossAttn}(\text{Cat}(\text{SelfAttn}(f_t, t_{text}), t_p), f_v). \quad (9)$$

After obtaining the t'_{text} , we re-project and append it into the visual prompt tokens t_p by an MLP to form the enhanced prompt tokens $t'_p = [t_p, \text{MLP}(t'_{text})]$ for improving binary segmentation. Notice the semantic-aware decoder has already the ground truth semantic labels, it uses t_p instead of t'_p , as it is empirically unnecessary.

3.3. Model Learning

We train the SEG-SAM by simulating the interactive approach following [12, 22]: during training, we randomly select 5 foreground objects in each image to form a training batch, and randomly pick points or one box for each object for prompting; for inference, we randomly select one foreground object for segmentation and generate one corresponding point or box as visual prompt. In addition, we can flexibly adjust SEG-SAM for different inference tasks. For binary medical segmentation, we use SEG-SAM’s Dec_{sag} to produce binary masks. For semantic medical segmentation, we use the output of the Dec_{saw} instead. Next, we introduce the cross-mask spatial alignment and then provide the overall training loss of SEG-SAM.

Cross-mask spatial alignment. In our method, the two decoders of SEG-SAM learn complementary representations: Dec_{saw} focuses on semantic differences between object categories, while Dec_{sag} emphasizes separating foreground object from background. Based on it, we propose the cross-mask spatial alignment to establish the mask consistency on the same prompted object O_p . Specifically, given the semantic mask M_s from Dec_{saw} with semantic labels being

stripped off and binary mask M_b from Dec_{sag} , we compute their interaction over union (IoU) and write the loss as minimizing $1 - \text{IoU}$ (theoretically, their IoU should be 1). The proposed loss can be written as:

$$\mathcal{L}^{cons} = 1 - \frac{|M_s \cap M_b|}{|M_s \cup M_b|}. \quad (10)$$

Overall loss. We use the binary segmentation loss \mathcal{L}^{bin} in Dec_{sag} , including the focal loss \mathcal{L}^{focal} and Dice loss \mathcal{L}^{dice} [22]. In Dec_{saw} , we introduce the semantic learning including both semantic mask prediction P_{mask} and semantic classification P_{cat} : for P_{mask} , we employ the semantic segmentation loss \mathcal{L}^{sem} [11], consisting of the cross entropy loss \mathcal{L}^{ce} and segmentation loss \mathcal{L}^{dice} ; for P_{cat} , we use the binary cross entropy loss \mathcal{L}^{bce} for supervision.

The overall loss function of SEG-SAM can be written as:

$$\mathcal{L} = \mathcal{L}^{bin} + \mathcal{L}^{sem} + \mathcal{L}^{cons} + \lambda \mathcal{L}^{bce}, \quad (11)$$

where the λ is the loss weight of \mathcal{L}^{bce} .

4. Experiments

4.1. Experiments setup

Datasets. Our experiments are conducted on the Med2D-16M dataset [12]. It is recognized as the largest publicly available benchmark for medical segmentation, which consists of 8 modalities and about 200 categories, with a total of 3.6M images and 16M annotated masks. We split all image data into an 80% training set and a 20% testing set. Due to our limited computational resources (*i.e.*, four 4090 GPUs for all experiments), we utilize a 1/4 subset of the training set to train our method and all comparable methods on the Med2D-16M dataset, while use the whole testing set to evaluate the medical segmentation performance of these methods. To evaluate the generalization of our SEG-SAM, we conduct cross-dataset experiments on 3 new datasets that are not incorporated in Med2D-16M, including the KiTS23 [17], BTCV [23], and AMOS [19] datasets.

Data pre-processing. For data pre-processing, we apply the same pre-processing approach in SAM-Med2D [12]. Specifically, for 3D image data, we extract all slice images along the three axes and convert them into 2D images [12]. For 2D image data, we only ensure all pixel values are within the range of $[0, 255]$. Next, we remove ground-truth masks of an image proportion of less than 0.153% ($\frac{100}{256 \times 256}$), as they are too small to extract [12].

Evaluation metrics. We use the widely adopted Dice Similarity Coefficient (DSC, also named DICE) in previous methods [12, 28] to evaluate the binary segmentation performance of our method. In addition, to comprehensively evaluate SEG-SAM’s semantic segmentation performance, we employ the widely used mean DICE (mDSC) across modalities [8, 23, 43] in semantic medical segmentation.

Method	Prompt	CT	MR	PET	Derm.	Endo.	Fund.	Ultr.	X-ray	Avg.
SAM [22]	Point	28.89	22.47	35.38	35.81	31.40	30.02	18.94	19.58	27.81
FT-SAM [22]		48.96	33.13	21.97	82.17	39.35	61.15	32.10	25.16	43.00
FT-SAM2 [30]		61.33	42.61	70.01	82.84	57.05	72.46	63.68	45.00	61.87
SAM-Med2D [12]		70.35	47.72	72.03	85.97	58.87	75.63	64.84	48.18	65.45
MedSAM [28]		72.86	50.58	68.27	86.21	54.61	76.43	68.41	52.63	66.25
Med-SA [34]		72.31	46.67	72.45	88.54	58.91	77.55	65.50	41.29	65.40
Ours		79.23	54.79	78.60	89.37	69.74	81.47	71.77	60.25	73.15
SAM [22]	Box	63.49	50.82	63.01	83.57	69.72	76.95	76.47	51.98	67.00
FT-SAM [22]		79.35	59.13	75.53	90.25	77.18	84.23	79.35	59.07	75.51
FT-SAM2 [30]		78.49	58.68	76.89	90.86	77.70	85.74	84.34	60.24	76.62
SAM-Med2D [12]		80.57	60.49	78.38	92.30	76.60	86.49	84.89	58.65	77.30
MedSAM [28]		82.60	62.92	76.99	90.85	73.72	83.91	84.73	63.24	77.37
Med-SA [34]		82.82	61.19	79.29	92.56	76.42	85.38	83.53	56.64	77.23
Ours		86.09	66.31	82.63	92.64	81.73	85.61	86.00	70.70	81.46

Table 1. Comparison between our method and other state-of-the-art SAM-based methods on the Med2D-16M dataset. We use the DICE to evaluate the binary medical segmentation performance.

Method	Prompt	CT	MR	PET	Derm.	Endo.	Fund.	Ultr.	X-ray	Avg.
nnUNet [18]	-	55.00	40.70	52.01	46.79	45.35	9.02	26.81	42.35	39.75
UNETR [16]		42.97	44.35	0.00	81.83	59.35	11.76	36.62	50.43	40.91
nnFormer [42]		49.59	47.18	52.89	77.14	35.97	33.43	47.18	57.78	50.15
U-Mamba [29]		57.89	51.59	55.06	75.58	44.55	18.84	46.01	55.00	50.57
Med2D* [12]	Point	55.44	41.47	69.16	83.12	68.86	68.67	68.27	79.27	66.78
MedSAM* [28]		51.30	43.65	72.40	86.23	56.57	80.55	62.77	67.93	65.18
Med-SA* [34]		49.69	42.19	71.32	90.60	56.64	89.61	73.63	81.39	69.38
Ours		62.62	51.47	79.24	88.69	70.22	94.98	70.32	84.69	75.28
Med2D* [12]	Box	56.28	49.94	81.07	94.34	70.95	90.04	87.00	83.29	76.61
MedSAM* [28]		58.71	56.15	77.46	90.72	64.77	88.83	85.43	76.17	74.78
Med-SA* [34]		58.46	55.62	80.15	90.88	69.87	88.25	85.71	83.13	76.51
Ours		69.88	63.40	84.17	91.63	79.87	90.39	87.16	80.71	80.90

Table 2. Comparison between our method and other state-of-the-art SAM-based methods on the Med2D-16M dataset. We use the mDSC to evaluate the semantic medical segmentation performance. * indicates that we integrate our semantic-aware decoder into them.

Implementation details. In all experiments, we use 4 NVIDIA 4090 GPUs to train SEG-SAM and other methods and use each GPU to process 32 images. All input images are resized to 256×256 pixels. We adopt the Adam optimizer [21] with an initial learning rate of $1e^{-4}$. We train SEG-SAM for 15 epochs, and reduce the learning rate by half at 5-th and 10-th epochs. Following SAM-Med2D [12], we randomly select 5 corresponding masks in each image for training. For the image decoder, we use the pre-trained ViT-B/16 from SAM [22] as the backbone and freeze its original parameters. For the prompt encoder and mask decoder, we adopt SAM’s configuration and update their parameters during model training. We empirically set $\lambda = 10$.

4.2. Unified Semantic Segmentation

Unified binary medical segmentation. We first explore the binary medical segmentation performance of our method on Med2D-16M dataset. In Table 1, we compare our SEG-

SAM with vanilla SAM [22] without fine-tuning and its updated version with fine-tuning (FT-SAM). We further compare with the enhanced SAM2 model [15]. We also compare with three state-of-the-art SAM-based methods, including the SAM-Med2D [12], MedSAM [28], and Med-SA [34]. All these methods are implemented following their publicly available code-base and applied the same interactive training approach through point or bounding box prompt. We employ the DSC metric to evaluate the binary medical segmentation performance across 8 modalities and further report the average DSC in all modalities.

As demonstrated by the results, our method significantly outperforms other SAM-based methods across seven modalities (CT, MR, PET, etc). Especially, our method achieves significantly better results in the average DSC under both point and box prompts. This strongly demonstrates the importance of our semantic learning strategy for unified binary medical segmentation.

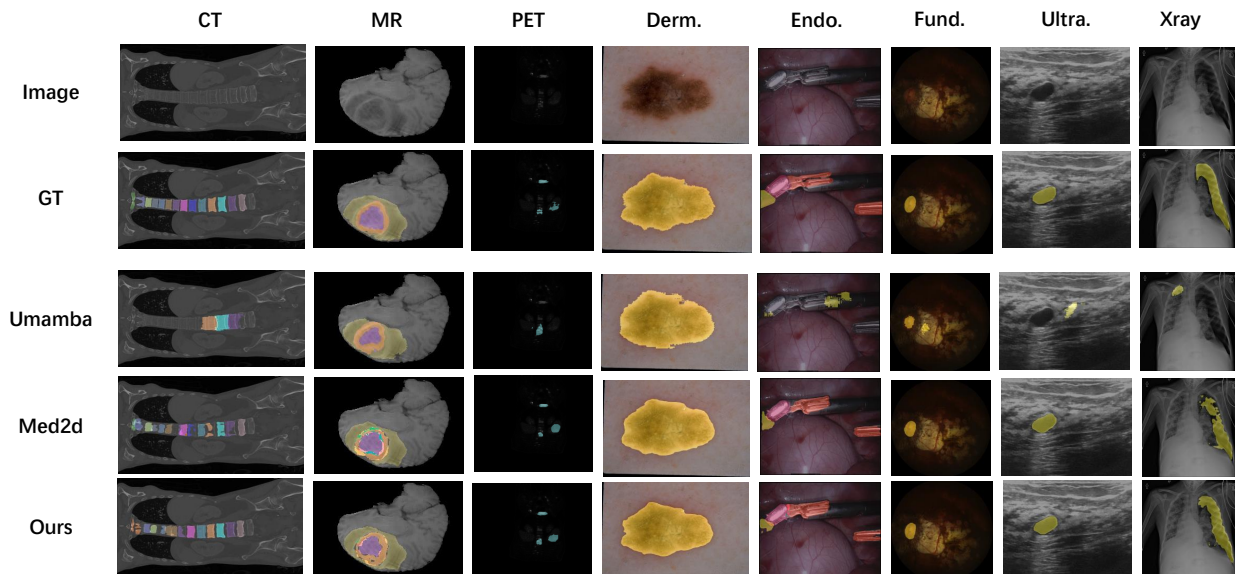


Figure 3. Qualitative comparisons with other methods on 8 modalities. We compared with U-Mamba [29] and Med2D [12]

Method	KiTS	BTCV	AMOS
nnU-net [18]	34.15	17.69	28.69
UNETR [16]	47.80	13.60	15.63
nnFormer [42]	45.27	17.90	26.95
U-Mamba [29]	53.74	20.95	29.58
Med2D* [12]	72.34	64.83	62.01
MedSAM* [28]	70.50	59.03	50.85
Med-SA* [34]	71.79	59.43	51.54
Ours	74.18	71.54	68.33

Table 3. Comparison with other SAM-based methods that integrated with ours. * indicates that we integrate our semantic-aware decoder with them.

Unified semantic medical segmentation. We further evaluate the semantic segmentation performance of our method on Med2D-16M dataset. In Table 2, we compare SEG-SAM with the conventional medical segmentation methods, including the nnU-net [18], UNETR [16], nnFormer [42] and U-Mamba [29]. For a fair comparison, we train these methods using the same setup as our method on the Med2D-16M dataset. In addition, we integrate the proposed semantic learning strategy into these SAM-based method to perform semantic prediction. We employ the mDSC metric to evaluate the performance of all methods across 8 modalities and report the average mDICE. The results indicate that our method significantly outperforms conventional task-specific methods [16, 18, 29, 42] and other SAM-based methods [12, 28, 34] in unified semantic medical segmentation. In addition, the SAM-based method integrated with our se-

mantic learning strategy (denoted as method_{*}) demonstrate superior performance compared to conventional methods [16, 18, 29, 42]. The main reason is that our proposed semantic-guided learning can effectively leverage semantic learning to transfer SAM’s representation capabilities from natural domains to medical segmentation tasks, enabling accurate semantic segmentation of diverse medical objects.

Cross dataset experiments. We employ new 3 datasets that their classes are not involved in Med2D-16M dataset at all, including the KiTS23 [17], BTCV [23], and AMOS [19] datasets, to evaluate the generalization of our method. In Table 3, we test the trained model from Med2D-16M on three datasets. All comparable methods are trained in the same way. The results demonstrate very good generalizability of our method compared to others.

Visualization results. In Fig. 3, we visualize the semantic segmentation results of our method on the SA-Med2D-16M dataset, compared with other SAM-based (e.g., Med2D [12]) and task-specific (e.g., U-Mamba [29]) approaches.

4.3. Ablation Study

We conduct the ablation study on Med2D-16M dataset to evaluate different components of our SEG-SAM. Specifically, we remove the semantic-aware decoder and text-to-visual semantic enhancement module, so that a vanilla SAM-Med2D serves as our baseline for binary segmentation. Additionally, we introduce a cls token in SAM-Med2D’s original mask decoder to directly turn it into a semantic decoder, serving as another baseline for semantic segmentation. We use the box prompt by default for all ablation study.

Semantic-aware Decoder. To evaluate our Semantic-aware

Method	SAWD _{pmt}	SAWD _{unpmt}	Components			Med2D	
			SAWD _{sem}	T2VSE	CMSA-Loss	DSC	mDSC
Baseline						77.30	-
Baseline _{sem}						74.72	76.35
1)	✓					78.01	78.83
2)	✓	✓				78.61	79.34
3)	✓		✓			77.03	77.61
4)	✓	✓		✓		80.13	80.35
SEG-SAM	✓	✓		✓	✓	81.46	80.90

Table 4. The ablation study of our method on Med2D-16M datasets. We take the vanilla SAM as our baseline for binary segmentation, while introducing an additional classification token in SAM’s decoder as another baseline for semantic segmentation. Afterwards, we add each of our components to the baseline to observe performance improvement both binary and semantic segmentation.

Method	Med2D		KiTS		BTCV		
	DSC	mDSC	DSC	mDSC	DSC	mDSC	
Med2D	Ori.	77.30	-	86.69	-	81.80	-
	Aft.	78.51	76.61	87.13	72.34	83.47	64.83
MedSAM	Ori.	77.37	-	85.56	-	82.60	-
	Aft.	78.83	74.78	86.75	70.50	83.92	59.03
Med-SA	Ori.	77.23	-	85.78	-	81.20	-
	Aft.	78.42	76.51	86.84	71.79	85.24	59.43

Table 5. We integrate our semantic-aware decoder into other SAM-based methods and report on the DSC and mDSC metrics. Ori. means their original performance, Aft. means these methods integrated with our SAWD.

Decoder in Table 4. We first add the semantic-oriented token in the decoder SAWD_{pro} for only the prompted object’s segmentation. Then we add the classification-oriented tokens in SAWD_{unpro} for unprompted objects’ classification. Results indicate that our SAWD_{pro} could bring the semantic prediction capability to SAM and also improve its binary segmentation performance. SAWD_{unpro} further enhances the performance. Overall, our SAWD leads to increase in DSC by 3.89 and in mDSC by 2.99 compared to Baseline_{sem}. Besides, we design an alternative variant of SAWD_{fsem}, which performs full image semantic segmentation on all objects. As showed in Table 4 line 3), it results in a performance drop in both binary and semantic segmentation. This demonstrates that this costly way indeed can not easily configured well with the semantic segmentation task on the prompted object, due to conflicts they may have.

Text-to-Vision Semantic Enhancement. To validate the effect of text-to-vision semantic enhancement scheme, we ablate it in Table 4. Results show that our T2VSE could increase the both the binary result and semantic results, brings an increase of DSC by 1.52 and mDSC by 1.01.

Cross-mask Spatial Alignment. To evaluate the impact of cross-mask spatial alignment, we remove the loss \mathcal{L}^{cons} from Eq. 11 for model training. We discover that this loss

clearly benefits the model for both binary and semantic segmentation performance. As shown in Table 4, removing this loss leads to decrease in DSC by 1.33 and mDSC by 0.55.

Integration with other SAM-based methods. To validate the plug-in ability of our SEG-SAM, we integrate the semantic-aware decoder into other SAM-based methods. As illustrated in Table 5, these methods integrated with the semantic learning achieve higher DSE scores across four datasets for both binary and semantic segmentation performance. Of course they are still inferior to our SEG-SAM, due to their different finetuning strategies and lack of medical text knowledge. The results demonstrating our method could bring the semantic prediction capability into the SAM family for improving both binary segmentation and introducing the semantic segmentation.

5. Conclusion

In this work, we introduce SEMantic-Guided SAM (SEG-SAM), a unified model designed to improve the medical segmentation performance by incorporating semantic knowledge into the SAM framework. We first develop a semantic-aware decoder that complements SAM’s original semantic-agnostic decoder, enabling the model to handle both binary and semantic segmentation tasks within medical images. By integrating text-to-vision semantic enhancement scheme, SEG-SAM leverages detailed category-specific knowledge from the large language model and use it to improve the binary segmentation accuracy. Additionally, we propose a cross-mask spatial alignment strategy to encourage consistency between the outputs of the two decoders, further strengthening the segmentation precision. Extensive experiments on multiple public datasets demonstrate that SEG-SAM not only outperforms SAM-based models in binary segmentation but also offers a significant advantage in semantic segmentation task. Future work will extend this approach to medical video domains and refining the integration of language-driven semantics.

References

- [1] Josh Achiam, Steven Adler, Sandhini Agarwal, Lama Ahmad, Ilge Akkaya, Florencia Leoni Aleman, Diogo Almeida, Janko Altenschmidt, Sam Altman, Shyamal Anadkat, et al. Gpt-4 technical report. *arXiv preprint arXiv:2303.08774*, 2023. 2, 5, 1
- [2] Reza Azad, Ehsan Khodapanah Aghdam, Amelie Rauland, Yiwei Jia, Atlas Haddadi Avval, Afshin Bozorgpour, Sanaz Karimijafarbigloo, Joseph Paul Cohen, Ehsan Adeli, and Dorit Merhof. Medical image segmentation review: The success of u-net. *IEEE Transactions on Pattern Analysis and Machine Intelligence*, 2024. 2
- [3] Victor Ion Butoi, Jose Javier Gonzalez Ortiz, Tianyu Ma, Mert R Sabuncu, John Guttag, and Adrian V Dalca. Universeg: Universal medical image segmentation. In *Proceedings of the IEEE/CVF International Conference on Computer Vision*, pages 21438–21451, 2023. 1
- [4] Victor Ion Butoi, Jose Javier Gonzalez Ortiz, Tianyu Ma, Mert R Sabuncu, John Guttag, and Adrian V Dalca. Universeg: Universal medical image segmentation. In *Proceedings of the IEEE/CVF International Conference on Computer Vision*, pages 21438–21451, 2023. 2
- [5] Hu Cao, Yueyue Wang, Joy Chen, Dongsheng Jiang, Xiaopeng Zhang, Qi Tian, and Manning Wang. Swin-unet: Unet-like pure transformer for medical image segmentation. In *European conference on computer vision*, pages 205–218. Springer, 2022. 2
- [6] Jiazhong Cen, Zanwei Zhou, Jiemin Fang, Wei Shen, Lingxi Xie, Dongsheng Jiang, Xiaopeng Zhang, Qi Tian, et al. Segment anything in 3d with nerfs. *Advances in Neural Information Processing Systems*, 36:25971–25990, 2023. 2
- [7] Jieneng Chen, Jeru Mei, Xianhang Li, Yongyi Lu, Qihang Yu, Qingyue Wei, Xiangde Luo, Yutong Xie, Ehsan Adeli, Yan Wang, et al. Transunet: Rethinking the u-net architecture design for medical image segmentation through the lens of transformers. *Medical Image Analysis*, 97:103280, 2024. 2
- [8] Liang-Chieh Chen, George Papandreou, Iasonas Kokkinos, Kevin Murphy, and Alan L Yuille. Deeplab: Semantic image segmentation with deep convolutional nets, atrous convolution, and fully connected crfs. *IEEE transactions on pattern analysis and machine intelligence*, 40(4):834–848, 2017. 5
- [9] Shoufa Chen, Chongjian Ge, Zhan Tong, Jiangliu Wang, Yibing Song, Jue Wang, and Ping Luo. Adaptformer: Adapting vision transformers for scalable visual recognition. *Advances in Neural Information Processing Systems*, 35:16664–16678, 2022. 1
- [10] Xuxin Chen, Ximin Wang, Ke Zhang, Kar-Ming Fung, Theresa C Thai, Kathleen Moore, Robert S Mannel, Hong Liu, Bin Zheng, and Yuchen Qiu. Recent advances and clinical applications of deep learning in medical image analysis. *Medical image analysis*, 79:102444, 2022. 1
- [11] Bowen Cheng, Ishan Misra, Alexander G Schwing, Alexander Kirillov, and Rohit Girdhar. Masked-attention mask transformer for universal image segmentation. In *Proceedings of the IEEE/CVF conference on computer vision and pattern recognition*, pages 1290–1299, 2022. 5
- [12] Junlong Cheng, Jin Ye, Zhongying Deng, Jianpin Chen, Tianbin Li, Haoyu Wang, Yanzhou Su, Ziyang Huang, Jilong Chen, Lei Jiang, et al. Sam-med2d. *arXiv preprint arXiv:2308.16184*, 2023. 3, 5, 6, 7
- [13] Alexey Dosovitskiy. An image is worth 16x16 words: Transformers for image recognition at scale. *arXiv preprint arXiv:2010.11929*, 2020. 2, 3
- [14] Yunhe Gao. Training like a medical resident: Context-prior learning toward universal medical image segmentation. In *Proceedings of the IEEE/CVF Conference on Computer Vision and Pattern Recognition*, pages 11194–11204, 2024. 2
- [15] Simon Graham, Quoc Dang Vu, Mostafa Jahanifar, Shan E Ahmed Raza, Fayyaz Minhas, David Snead, and Nasir Rajpoot. One model is all you need: multi-task learning enables simultaneous histology image segmentation and classification. *Medical Image Analysis*, 83:102685, 2023. 1, 6
- [16] Ali Hatamizadeh, Yucheng Tang, Vishwesh Nath, Dong Yang, Andriy Myronenko, Bennett Landman, Holger R Roth, and Daguang Xu. Unetr: Transformers for 3d medical image segmentation. In *Proceedings of the IEEE/CVF winter conference on applications of computer vision*, pages 574–584, 2022. 6, 7
- [17] Nicholas Heller, Fabian Isensee, Dasha Trofimova, Resha Tejpal, Zhongchen Zhao, Huai Chen, Lisheng Wang, Alex Golts, Daniel Khapun, Daniel Shats, et al. The kits21 challenge: Automatic segmentation of kidneys, renal tumors, and renal cysts in corticomedullary-phase ct. *arXiv preprint arXiv:2307.01984*, 2023. 5, 7
- [18] Fabian Isensee, Paul F Jaeger, Simon AA Kohl, Jens Petersen, and Klaus H Maier-Hein. nnu-net: a self-configuring method for deep learning-based biomedical image segmentation. *Nature methods*, 18(2):203–211, 2021. 6, 7
- [19] Yuanfeng Ji, Haotian Bai, Chongjian Ge, Jie Yang, Ye Zhu, Ruimao Zhang, Zhen Li, Lingyan Zhanng, Wanling Ma, Xiang Wan, et al. Amos: A large-scale abdominal multi-organ benchmark for versatile medical image segmentation. *Advances in neural information processing systems*, 35:36722–36732, 2022. 2, 5, 7
- [20] Lei Ke, Mingqiao Ye, Martin Danelljan, Yu-Wing Tai, Chi-Keung Tang, Fisher Yu, et al. Segment anything in high quality. *Advances in Neural Information Processing Systems*, 36, 2024. 2
- [21] Diederik P Kingma. Adam: A method for stochastic optimization. *arXiv preprint arXiv:1412.6980*, 2014. 6
- [22] Alexander Kirillov, Eric Mintun, Nikhila Ravi, Hanzi Mao, Chloe Rolland, Laura Gustafson, Tete Xiao, Spencer Whitehead, Alexander C Berg, Wan-Yen Lo, et al. Segment anything. In *Proceedings of the IEEE/CVF International Conference on Computer Vision*, pages 4015–4026, 2023. 1, 2, 3, 5, 6
- [23] Bennett Landman, Zhoubing Xu, J Igelsias, Martin Styner, Thomas Langerak, and Arno Klein. Miccai multi-atlas labeling beyond the cranial vault—workshop and challenge. In *Proc. MICCAI Multi-Atlas Labeling Beyond Cranial Vault—Workshop Challenge*, page 12, 2015. 5, 7
- [24] Jie Liu, Yixiao Zhang, Kang Wang, Mehmet Can Yavuz, Xiaoxi Chen, Yixuan Yuan, Haoliang Li, Yang Yang, Alan

- Yuille, Yucheng Tang, et al. Universal and extensible language-vision models for organ segmentation and tumor detection from abdominal computed tomography. *Medical Image Analysis*, page 103226, 2024. 2
- [25] Ze Liu, Yutong Lin, Yue Cao, Han Hu, Yixuan Wei, Zheng Zhang, Stephen Lin, and Baining Guo. Swin transformer: Hierarchical vision transformer using shifted windows. In *Proceedings of the IEEE/CVF international conference on computer vision*, pages 10012–10022, 2021. 2
- [26] Jonathan Long, Evan Shelhamer, and Trevor Darrell. Fully convolutional networks for semantic segmentation. In *Proceedings of the IEEE conference on computer vision and pattern recognition*, pages 3431–3440, 2015. 2
- [27] Timo Lüddecke and Alexander Ecker. Image segmentation using text and image prompts. In *Proceedings of the IEEE/CVF conference on computer vision and pattern recognition*, pages 7086–7096, 2022. 1
- [28] Jun Ma, Yuting He, Feifei Li, Lin Han, Chenyu You, and Bo Wang. Segment anything in medical images. *Nature Communications*, 15(1):654, 2024. 1, 2, 5, 6, 7
- [29] Jun Ma, Feifei Li, and Bo Wang. U-mamba: Enhancing long-range dependency for biomedical image segmentation. *arXiv preprint arXiv:2401.04722*, 2024. 6, 7
- [30] Nikhila Ravi, Valentin Gabeur, Yuan-Ting Hu, Ronghang Hu, Chaitanya Ryali, Tengyu Ma, Haitham Khedr, Roman Rädle, Chloe Rolland, Laura Gustafson, et al. Sam 2: Segment anything in images and videos. *arXiv preprint arXiv:2408.00714*, 2024. 6
- [31] Simiao Ren, Francesco Luzi, Saad Lahrchi, Kaleb Kassaw, Leslie M Collins, Kyle Bradbury, and Jordan M Malof. Segment anything, from space? In *Proceedings of the IEEE/CVF Winter Conference on Applications of Computer Vision*, pages 8355–8365, 2024. 2
- [32] Olaf Ronneberger, Philipp Fischer, and Thomas Brox. U-net: Convolutional networks for biomedical image segmentation. In *Medical image computing and computer-assisted intervention—MICCAI 2015: 18th international conference, Munich, Germany, October 5-9, 2015, proceedings, part III 18*, pages 234–241. Springer, 2015. 2
- [33] A Vaswani. Attention is all you need. *Advances in Neural Information Processing Systems*, 2017. 2, 4
- [34] Junde Wu, Wei Ji, Yuanpei Liu, Huazhu Fu, Min Xu, Yanwu Xu, and Yueming Jin. Medical sam adapter: Adapting segment anything model for medical image segmentation. *arXiv preprint arXiv:2304.12620*, 2023. 3, 6, 7
- [35] Bin Xie, Hao Tang, Bin Duan, Dawen Cai, and Yan Yan. Maskam: Towards auto-prompt sam with mask classification for medical image segmentation. *arXiv preprint arXiv:2403.14103*, 2024. 3
- [36] Yiwen Ye, Yutong Xie, Jianpeng Zhang, Ziyang Chen, and Yong Xia. Uniseg: A prompt-driven universal segmentation model as well as a strong representation learner. In *International Conference on Medical Image Computing and Computer-Assisted Intervention*, pages 508–518. Springer, 2023. 1
- [37] Yiwen Ye, Yutong Xie, Jianpeng Zhang, Ziyang Chen, and Yong Xia. Uniseg: A prompt-driven universal segmentation model as well as a strong representation learner. In *International Conference on Medical Image Computing and Computer-Assisted Intervention*, pages 508–518. Springer, 2023. 2
- [38] Tao Yu, Runseng Feng, Ruoyu Feng, Jinming Liu, Xin Jin, Wenjun Zeng, and Zhibo Chen. Inpaint anything: Segment anything meets image inpainting. *arXiv preprint arXiv:2304.06790*, 2023. 2
- [39] Yao Zhang, Jiawei Yang, Jiang Tian, Zhongchao Shi, Cheng Zhong, Yang Zhang, and Zhiqiang He. Modality-aware mutual learning for multi-modal medical image segmentation. In *Medical Image Computing and Computer Assisted Intervention—MICCAI 2021: 24th International Conference, Strasbourg, France, September 27–October 1, 2021, Proceedings, Part I 24*, pages 589–599. Springer, 2021. 1
- [40] Chunpeng Zhou, Kangjie Ning, Qianqian Shen, Sheng Zhou, Zhi Yu, and Haishuai Wang. Sam-sp: Self-prompting makes sam great again. *arXiv preprint arXiv:2408.12364*, 2024. 1
- [41] Chunpeng Zhou, Kangjie Ning, Qianqian Shen, Sheng Zhou, Zhi Yu, and Haishuai Wang. Sam-sp: Self-prompting makes sam great again. *arXiv preprint arXiv:2408.12364*, 2024. 3
- [42] Hong-Yu Zhou, Jiansen Guo, Yinghao Zhang, Xiaoguang Han, Lequan Yu, Liansheng Wang, and Yizhou Yu. nn-former: Volumetric medical image segmentation via a 3d transformer. *IEEE Transactions on Image Processing*, 2023. 6, 7
- [43] Zongwei Zhou, Md Mahfuzur Rahman Siddiquee, Nima Tajbakhsh, and Jianming Liang. Unet++: Redesigning skip connections to exploit multiscale features in image segmentation. *IEEE transactions on medical imaging*, 39(6):1856–1867, 2019. 5
- [44] Zijian Zhou, Oluwatosin Alabi, Meng Wei, Tom Vercauteren, and Miaoqing Shi. Text promptable surgical instrument segmentation with vision-language models. *Advances in Neural Information Processing Systems*, 36:28611–28623, 2023. 1, 2
- [45] Xueyan Zou, Jianwei Yang, Hao Zhang, Feng Li, Linjie Li, Jianfeng Wang, Lijuan Wang, Jianfeng Gao, and Yong Jae Lee. Segment everything everywhere all at once. *Advances in Neural Information Processing Systems*, 36, 2024. 1

SEG-SAM: Semantic-Guided SAM for Unified Medical Image Segmentation

Supplementary Material

6. Appendix

In the supplementary material, we provide the additional ablation study of our method (Sec. 6.1) as well as the text template we have used (Sec. 6.2). Training setup is the same to the main paper.

6.1. More Ablation Study

To further validate the effectiveness of our method, below, we present more results regarding the text-to-vision semantic enhancement (T2VSE) scheme and the proposed SEG-SAM with point prompts.

Text-to-Vision Semantic Enhancement. In the paper, we mentioned by the end of Sec. 3.2.2 that, the enhanced prompt tokens we obtained from Eq. 9, *i.e.*, t'_p , is only used in the original decoder Dec_{sag} of SAM but not the semantic-aware decoder Dec_{saw} , as the latter leverages ground-truth medical semantic labels directly. To validate this empirically, we let Dec_{saw} also use t'_p for decoding, termed as T2VSE_{v1} in Table 6. It can be seen that this results into no further improvement compared to T2VSE by default, attesting our choice.

Method	Med2D	
	DSC	mDSC
T2VSE	80.13	80.35
T2VSE_{v1}	80.07	80.42

Table 6. More ablation study on the text-to-vision semantic enhancement (T2VSE) scheme.

Integration with Other Methods under Point Prompts.

Due to the space limit in the main paper, we present here the results by integrating our Dec_{saw} into other SAM-based methods under the point prompts. As shown in Table 7, this brings improvements for all settings, demonstrating the generalizability of our method.

Components in SEG-SAM under Point Prompts. We further evaluate the performance of different components of our SEG-SAM under point prompts in Table 8. Consistent with the ablation study in Table 4 in the paper, we use two baselines, one is the vanilla SAM-Med2D and the other is the SAM-Med2D with a cls token. We ablate several things: 1) the semantic-oriented token in semantic-aware decoder for prompted object’s semantic segmentation, denoted by SAWD_{pmt} ; 2) the classification-oriented token in semantic-aware decoder for unprompted objects’ classification, denoted by SAWD_{unpmt} ; 3) the SAWD_{unpmt} ’s al-

Method		Med2D		KiTS		BTCV	
		DSC	mDSC	DSC	mDSC	DSC	mDSC
Med2D	Ori.	65.45	-	74.85	-	71.66	-
	Aft.	69.23	68.78	76.98	64.06	73.52	60.24
MedSAM	Ori.	66.25	-	75.69	-	73.96	-
	Aft.	69.43	65.18	76.56	63.93	75.91	47.99
Med-SA	Ori.	65.40	-	76.37	-	72.14	-
	Aft.	68.90	69.38	77.13	49.21	75.74	47.32

Table 7. Integration of our semantic-aware decoder into other SAM-based methods under the point prompts. Ori. and Aft. mean before and after the integration, respectively.

ternative variant, *i.e.* performing semantic segmentation for unprompted objects, denoted by SAWD_{sem} ; 4) the text-to-vision semantic enhancement (T2VSE) scheme for incorporating the medical text knowledge; and 5) the cross-mask spatial alignment loss for establishing the mask consistency. The experimental results clearly demonstrate the effectiveness of adding different components to the baseline, improving both binary and semantic segmentation. This, together with Table 4 in the paper, conclude the overall effectiveness of our SEG-SAM under both point and box prompts.

6.2. Text Template for Medical Text Description

In this section, we provide the text template for generating medical text descriptions from GPT-4 [1]. Specifically, we input a question to enable GPT-4 to generate the descriptions for the $[class_name]$, while also feeding an object class example highlighted in an image as a visual reference, to assist in the description generation process. The input question for GPT-4 is defined as:

Prompt: *Please directly describe the texture, shape, and position characteristics of the $[class_name]$ without making any medical diagnoses. The highlighted $[class_name]$ example in the image is available for additional reference. Your responses will not be used for any medical diagnosis or commercial purposes. Below is the answer format:*

1. *Texture: $[Description]$.*
 2. *Shape: $[Description]$.*
 3. *Positional: $[Description]$.*
-

Method	SAWD _{pmt}	SAWD _{unpmt}	Components			Med2D	
			SAWD _{sem}	T2VSE	CMSA-Loss	DSC	mDSC
Baseline						65.45	-
Baseline _{sem}						64.56	65.11
1)	✓					68.53	70.14
2)	✓	✓				69.88	71.68
3)	✓		✓			67.69	69.03
4)	✓	✓		✓		71.70	73.67
SEG-SAM	✓	✓		✓	✓	73.15	75.28

Table 8. The ablation study of our method (point prompts) on Med2D-16M datasets. We take the vanilla SAM as our baseline for binary segmentation, while introducing an additional classification token in SAM’s decoder as another baseline for semantic segmentation. Afterwards, we add each of our components to the baseline to observe performance improvement both binary and semantic segmentation.

Based on this text template, we generate the text descriptions for all medical categories, and present several examples below:

Heart Myocardium. *Texture: Texture characteristics of the heart myocardium is generally seen as a thick, rounded structure with distinct chambers and walls. Shape: The shape of heart myocardium typically appears as a uniform, striated texture due to the arrangement of muscle fibers. Position: The heart myocardium is located centrally within the image, situated between two black regions (likely lung areas), slightly towards the top left quadrant.*

Aorta. *Texture: Texture characteristics of the aorta typically include a smooth and uniform appearance with some visible internal structures such as the intimal layer. Shape: The shape of the aorta is typically tubular with a slightly curved or elongated appearance. Position: The aorta is centrally located within the image, slightly towards the upper central region.*

Pancreas. *Texture: Texture characteristics of the pancreas include a homogeneous appearance with a slightly grainy texture due to the presence of small lobules and ducts. Shape: The shape of the pancreas is typically elongated and tadpole-like, with a tapered head and wider body/tail. The organ may also appear crescent-shaped or curved, depending on the individual’s anatomy and imaging angle. Position: The pancreas is located centrally within the abdominal cavity, horizontally oriented.*